A breakthrough hydrogen and oxygen utilization in a H_2-O_2 PEMFC stack with dead-ended anode and cathode

Lixin Fan[1], Lu Xing[2], Zhengkai Tu[1,*], Siew Hwa Chan[3]

[1]School of Energy and Power Engineering, Huazhong University of Science and Technology, Wuhan, 430074, China

[2]Mechanical and Construction Engineering, Northumbria University, Newcastle, UK

[3]Energy Research Institute, Nanyang Technological University, 50 Nanyang Avenue, 637553, Singapore

*Corresponding author: tzklq@hust.edu.cn

Abstract: Proton exchange membrane fuel cells (PEMFCs) have been wildly used for marine and aerospace applications as energy devices, where pure hydrogen and oxygen are fed into the two sides of the membrane electrode assembly (MEA). The release of unreacted hydrogen and oxygen not only reduces the efficiency of the system but also causes the serious problem of hydrogen starvation. For this reason, fuel flow driving devices and methods such as pumps, ejectors, and solenoid valves are designed to recycle this unused gas. However, even with these devices, the release of gas into the environment is still inevitable. Therefore, this paper introduces a novel method that solves these problems and mitigates gas emissions using a dead-ended anode and cathode (DEAC) system. Pressure difference is formed between the inlet and outlet of PEMFC by controlling the purge valve to remove water and recycle hydrogen during purging. The dynamic response characteristics of this system under different current densities, pressure differences, and purging intervals are experimentally investigated in detail. The results show that both the hydrogen and oxygen utilizations can reach 100% and the collection of generated water during gas purging can be achieved in the DEAC mode.

Keywords: PEMFC, Dead-ended, Hydrogen, Oxygen, Utilization, Water management

1 Introduction

Proton exchange membrane fuel cells (PEMFC) has been considered as one of the most promising energy converting devices that provide energy with high efficiency and zero emissions while requiring short start-up times. For this reason, they are widely used in automobile vehicles[1-4], stationary power generation[5, 6], marine [7, 8] and aerospace applications [9-11]. However, water management[12, 13] and fuel recirculation management[14-17] are two key challenges for PEMFCs. The percentage of consumed hydrogen that is converted to generate electricity and thermal energy is called fuel utilization, which is a degree to measure the efficiency of the utilization of the supplied hydrogen. A fuel utilization of 100% implies that the amount of hydrogen supplied into the anode is theoretically the same as that required for the electrochemical reactions. However, there is a high risk of fuel starvation due to unstable voltages and degradation at the outlet of a stack, which is caused by the accumulation of water, so called flooding[18]. Poor mass transport also occurs in the stack due to flooding [13, 19]. As the main product of a fuel cell system, water exists in all parts of the system's key components; therefore, it is important to well manage water transport to maintain the efficient and stable operation of PEMFCs. Two parameters defined by Tajiri et al. [20] have been introduced to measure water vapor removal in which one represents convective water removal and the other represents diffusive water removal. Additionally, pressure was found to be one of the dominant factors affecting water removal.

In H_2/O_2 PEMFC systems, pure hydrogen and oxygen are excessively fed into the

system to prevent fuel starvation caused by water flooding. More specifically, the rate of supplying gas is higher than the required rate during the reaction in order to remove the water by convective forces generated from the excess gas flow. To utilize the excess fuel, recirculation devices or methods[21-23] are required to re-circulate the unused gas back into the system to improve fuel efficiency. For this reason, the implementation of the dead-ended mode is required and can be achieved with a dead-ended anode (DEA) [24-28], dead-ended cathode(DEC) [29], and dead-ended anode and cathode(DEAC) [30-32], each of which is required in different situations. The DEA mode is designed to increase the consumption rate of hydrogen, resulting in an improvement in efficiency. Fresh hydrogen is circulated into the inlet of the anode by an ejector or a hydrogen pump while oxygen is released into the air, as shown in Figure 1(a) [33]. Han et al.[34] designed, fabricated, and tested a 15-kW H_2/air PEMFC stack by controlling the purge valve to remove water and recycle hydrogen instead of using hydrogen recirculation devices, achieving a fuel utilization more than 99.6%. A dead-ended anode is implemented in a study by Jian et al. [35] to investigate the effectiveness of gas purging to enhance stack performance. They assembled a PEMFC stack by connecting 40 cells with an active area of 68.5 cm^2 while ambient air with a relative humidity of 64% and a temperature of 21°C was provided to the stack with a fan. In their results, each voltage curve is mostly flat, but a sharp drop occurs when gas purging is conducted, resulting in the dehydration of the membrane and a decrease in pressure. Zhao et al.[27] explored the characteristics of voltage decay and net power output in a DEA-mode PEMFC and proved the effectiveness of a DEA in improving net power by 3%. Wang et al.[28]

established a quasi-2D model with hydrogen recirculation and verified the positive effects of self-humidification of hydrogen and the uniformity of current distribution. By implementing exhaust oxygen recirculation at the outlet of the cathode channel, Rodosik et al.[36] reported a positive effect of the humidification of gas in the DEC to improve humidity from 25% to 85% in automotive applications. Bozorgnezhad et al. et al[37] demonstrated the water distribution in the cathode channel through direct visualization and image processing and developed a two-phase flow model for the water distribution in the cathode channel. Choi et al.[29] applied the hydrogen pulsation effect to the outlet of the cathode channel to decrease the performance degradation rate and found that the purging intervals should be minimized to improve oxygen utilization.

In marine and aerospace applications, requirements on room and environment conditions limit the release of gas, necessitating the implementation of the DEAC mode. In these power systems, pure hydrogen and oxygen are fed into the anode and cathode without emitting gas or water to the external environment, avoiding the risk of severe hazards due to flooding and/or the accumulation of impurity gas. Compared with H_2/air PEMFCs, it is more difficult to remove water in dead-ended H_2/O_2 PEMFCs and improve fuel utilization since water and extra fuel can be removed from H_2/air PEMFCs to the surroundings by an excess of reactant. By using direct visualization to analyze the water management in a PEMFC with a dead-ended mode, Rahimi et al. [30] investigated how different designs of flow field affect the water distribution in the cathode and anode. Additionally, they selected the current density as the parameter that determines when to perform the purging to increase the utilization of hydrogen and

oxygen. Barzegari et al. [38] developed a mathematical model for a cascade H_2/O_2 PEMFC stack to reuse the excess hydrogen and oxygen with an integrated humidifier and separator to remove water in the DEAC mode. The stack was separated into two stages with the second stage using the exhaust gas from the first stage. Chen et al. [31] utilized time regulators to control the purging intervals and durations in a PEMFC implemented with DEAC and studied the performance degradation during operation. They divided the degradation process into three stages, which include dehydration, quasi-equilibrium, and flooding. Koski et al.[39] presented a method to understand the gas composition dynamics and how does it to decouple the fuel utilization and efficiency in a DEAC PEMFC system with a recirculation pump. Dirk et al.[40] designed and assembled a PEMFC system with ejector-based recirculation to improve hydrogen utilization efficiency and found that the designed system demonstrated a performance similar to that of conventional designs; however, the ejectors were not capable of overcoming the pressure drop at low power outputs. Jia et al.[41] mitigated hydrogen starvation in an open cathode system by adding an exit reservoir at the outlet of the anode to alleviate the hydrogen starvation. Alizadeh et al.[42] proposed a cascade PEMFC with a humidifier and separator to improve hydrogen and oxygen utilization. From the literature, however, it can be noted that strategies for improving fuel utilization in dead-ended mode have been focused on hydrogen recirculation, whereas fewer studies involve improving oxygen utilization to a higher level or even to 100%.

In this work, a novel method to improve the efficiency of the H_2/O_2 PEMFC by gas purging to remove water without consuming parasitic power using a kW-class PEMFC

system in DEAC mode is newly proposed. As shown in Figure 1(b), pure hydrogen and pure oxygen are used as reaction gases for the cathode and anode, respectively, and the excess gas is fully stored during the purging interval and reused during purging. Two transparent buffer tanks are utilized to store the unreacted gas, provide a reactant, and store the liquid water during operation. The dynamic characteristics of the PEMFC under various current densities, pressure differences, and purging intervals are tested and analyzed by experiment. The proposed DEAC system improves the hydrogen and oxygen utilization efficiency to 100% and reduces the rate of performance degradation due to water flooding by collecting the generated water.

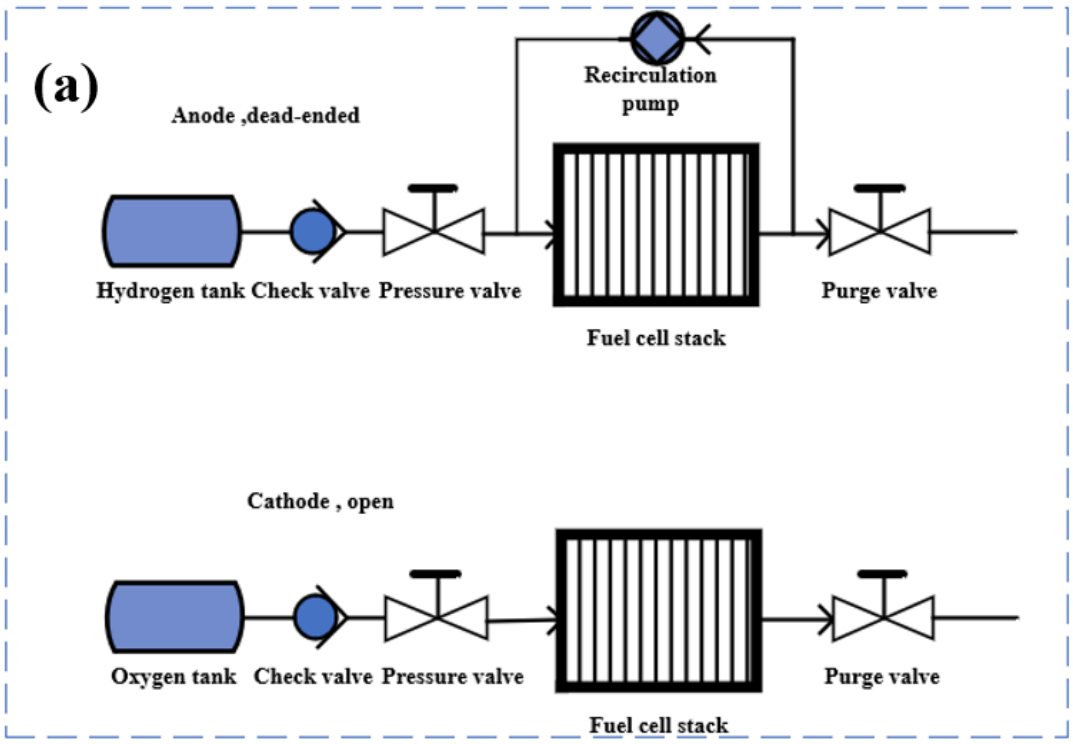

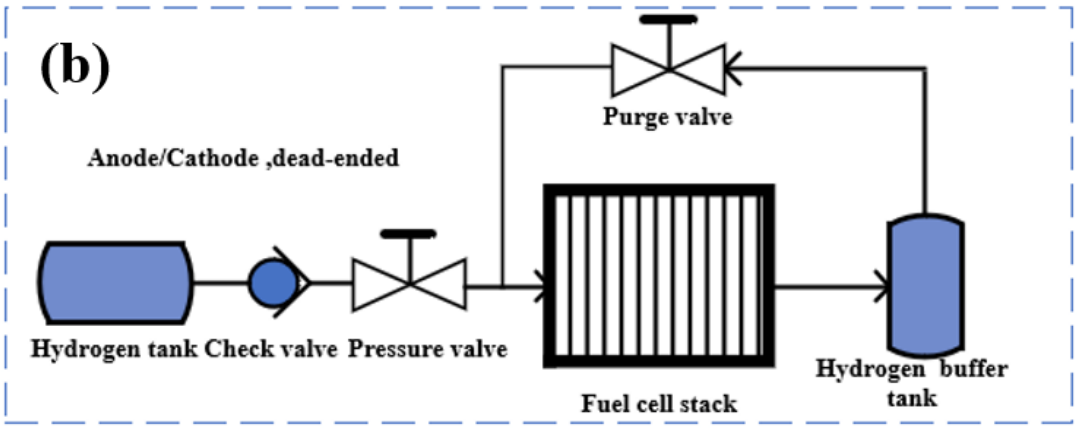

Figure 1. The comparison between normal dead-ended anode purging and our proposed DEAC purging: (a)Normal DEA purging and (b)Proposed DEAC purging methods.

2.Methods and materials

2.1 System Introductions

A H_2-O_2 PEMFC stack assembled with 10 cells has been designed and its parameters are shown in Table.1. Straight flow fields proposed in our former work[43] were used in this investigation and placed vertically to use gravity to improve water removal. The membrane electrode assembly (MEA) provided by WUT New Energy Company was fabricated through the catalyst coated membrane (CCM) technique with 0.4 mg·cm^{-2} Pt loading at two sides. The Nafion ® XL membrane from Dopont ™ was used as electrolyte.

The experiments were conducted on a kW-class test platform as shown in Figure 2. The system consists of four parts: a hydrogen supply subsystem, oxygen supply subsystem, cooling subsystem, and monitoring subsystem. As shown in Figure 2, the essential components of the system include two buffer tanks, an electronic load, a controlled purging subsystem, data acquisition instruments, and related sensors. The buffer tanks serve as a liquid separator to remove water and as a gas storage to store unused fuel.

Industrial PC (Adam 4150 and Adam 4017) served as data acquisition instruments to collect the data from sensors, including pressure with accuracy of 1kpa and error of ±0.25% and potential with accuracy of 1×10^{-4}V and error of ±0.5%, and feedback and control signals. Solenoid valves (AiTAC,2V025-08) are crucial for the monitoring and control system because they efficiently control the gas supply through their own opening and closing mechanism. The current density can be artificially controlled to meet the energy requirements of the electronic load.

The control strategy is shown in Figure 3 and conducted as following steps: 1) Initialize the controlling parameters, purging interval t_p, purging pressure P_l, and stop time t_s; 2) Initialize the purging time t_x;3) The solenoid valves at the inlet of the stack are open whereas those at the outlet of the buffer tanks are closed, indicating that the fresh reactants are served the gas source. 4) When the purging time t_x reaches the purging interval t_p, the solenoid valves at the outlet of the buffer tanks are open whereas those at the inlet of the stack are closed, indicating that the gas stored in the buffer tank is used as the gas source. 5) As the PEMFC consumes the fuel, the pressure for the system decreases due to the limited amount of gas. When the pressure drops to the purging pressure P_l, then step (2) is conducted and a new loop starts. The control strategy will be stopped until the total operating time reaches the set stop time t_s.

Table 1. Geometric parameters of the PEMFC stack

Parameters	Units	Value
Electrochemical active area	m^2	500×10^{-4}
Depth of channels	m	1×10^{-3}
Width of channels	m	2×10^{-3}
Width of ribs	m	2×10^{-3}
Thickness of gas diffusion layers	m	200×10^{-6}
Thickness of membranes	m	25×10^{-6}
Thickness of catalyst layer	m	10×10^{-6}

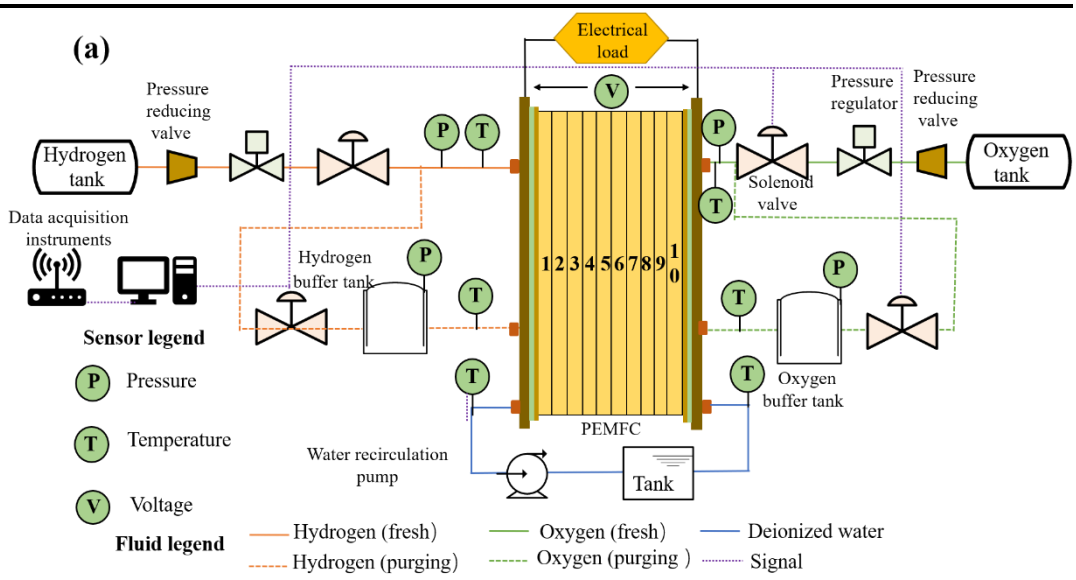

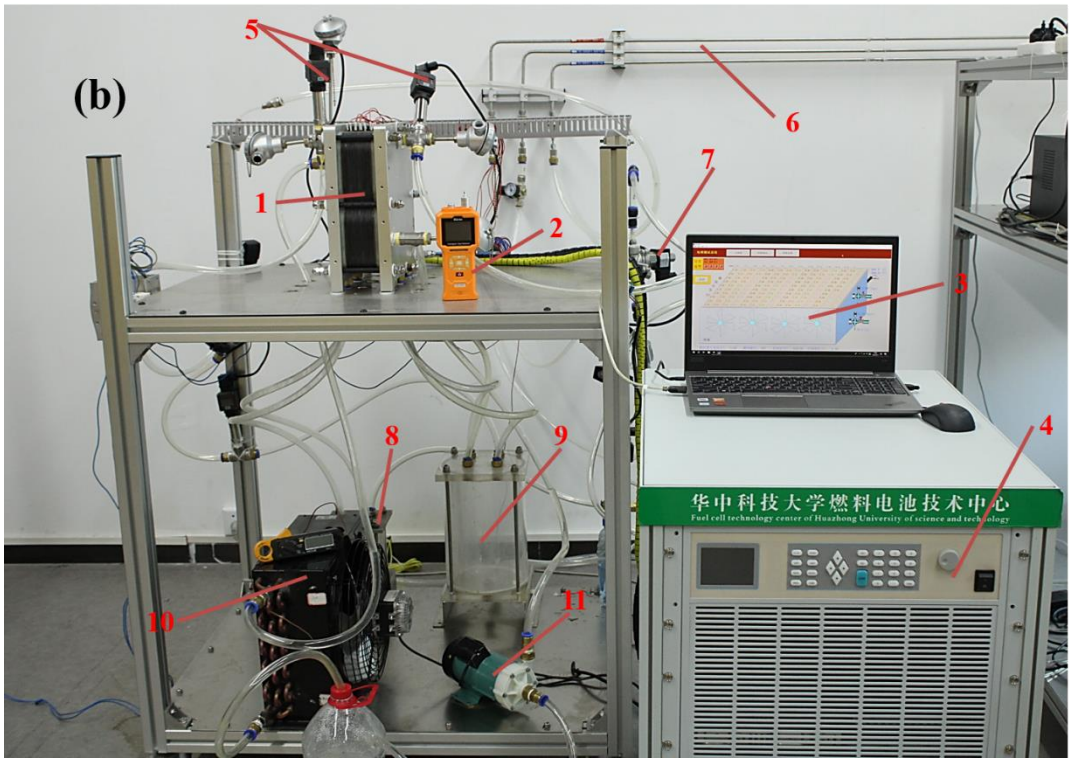

Figure 2. (a)The schematic of the overall system(b) The in-site scheme of test platform with 1kW PEMFC stack, 1-stack 2-hydrogen concentration alarm 3-Control interface 4-electrical load 5-presssor sensor 6-gas supply system (top to down, hydrogen, nitrogen and oxygen) 7- solenoid valve 8-hydrogen buffer tank 9-oxygen buffer tank 10-heat transfer 11-water pump

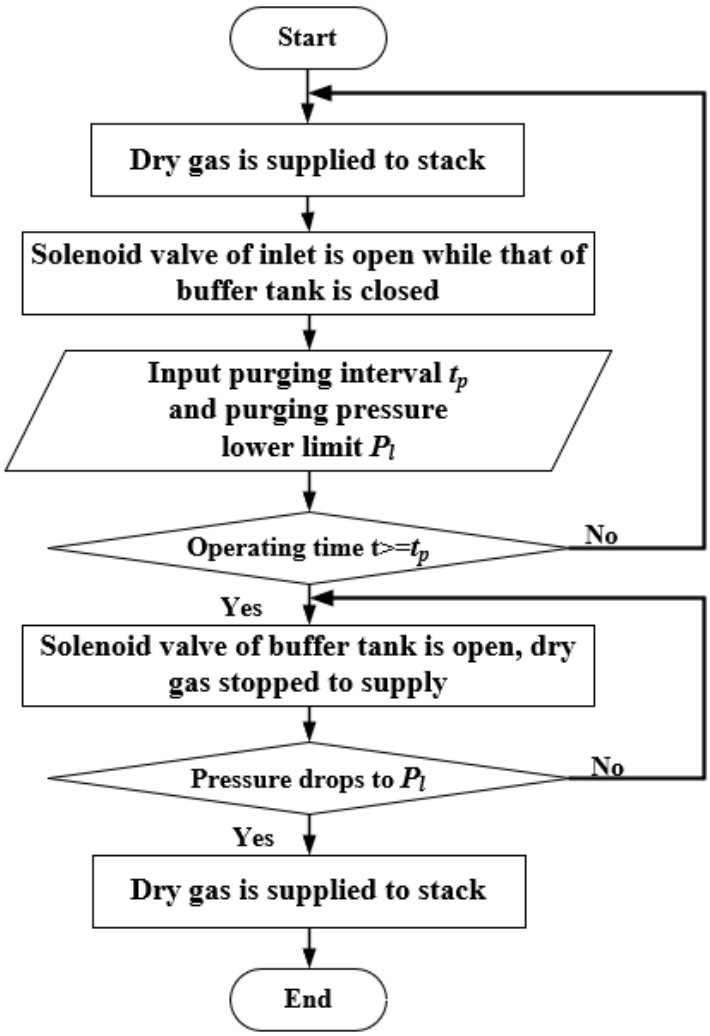

Figure. 3 Flow chart of time-pressure based purge process.

2.2 Experimental Procedure

To ensure the stable operation of the system, hydrogen with a purity of 99.999% as the fuel and 99.999% oxygen as the oxidant are fed through fixed regulator valves. The stack is activated by gradually loading current from 0 to the required current in steps of 2.5 A per minute to maintain stability and uniformity of the current density. When the output performance of the stack keeps stable, the control strategy as Figure 3 is conducted with recording the potential and pressure. To accurately measure and evaluate the performance of the PEMFC, the pressure and voltage data from these

sensors are recorded every second and temperature sensors are used to control the operating temperature of the system. Additionally, valves are installed at the bottom of the buffer tanks in case of an emergency.

2.3 Performance evaluation

According to Equations (1–8), the pressure difference and purging intervals are the key factors influencing water management during operation and, thereby, affect the performance of the PEMFC. The voltage of single cell V is strongly influenced by the pressure in the Nernst equation, which can be written as,

The output voltage of single cell V depends on the Nernst potential E_{nernst}, Ohmic overpotential V_{ohmic},activation overpotential V_{act}, and concentration overpotential V_{conc},

$$V=E_{\text{nernst}}-V_{\text{act}}-V_{\text{ohmic}}-V_{\text{conc}} \tag{1}$$

$$E_{\text{nernst}}=1.229-8.5\times10^{-3}(T_{ref}-298.15)+\frac{\text{R}T_{cell}}{2\text{F}}\ln[p^{*}_{H_2}(p^{*}_{O_2})^{0.5}] \tag{2}$$

$$V_{act}=-[\xi_1+\xi_2 T_{cell}+\xi_3 T_{cell}\ln C^{*}_{O_2}+\xi_4 T_{cell}\ln(\text{j}A_c)] \tag{3}$$

$$V_{ohm}=-jA_c(R_m+R_s) \tag{4}$$

$$V_{conc}=-b\ln(1-\frac{j}{j_{max}}) \tag{5}$$

where T_{cell} and T_{ref} are the operating and reference temperatures, respectively; and $p^{*}_{H_2}$ and $p^{*}_{O_2}$ are the partial pressures of hydrogen and oxygen, respectively. ξ_1, ξ_2, ξ_3, ξ_4, and b are empirical constants; j and j_{max} are the operating and maximum temperature current densities, respectively; R_{m} and R_{s} are the membrane and solid resistance, respectively; $C^{*}_{O_2}$ is the dissolved oxygen concentration; and A_c is the active area of the PEMFC.

In addition, dissolved oxygen concentration $C^{*}_{O_2}$ can be defined by Henry's law as

shown below.

$$C_{O_2}^{*} = \frac{p_{O_2}^{*}}{5.08\times10^{6} exp(-498/T_{cell})} \tag{6}$$

The membrane resistance was closely related to the water content in the electrolyte, as shown in the following expression [37].

$$R_m = \frac{1}{A_c} \frac{181.6(1+0.03j+0.062(T_{cell}/303)^2 \cdot j^{2.5})}{(\lambda-0.634-3j)\exp(4.18(T_{cell}-303)/T_{cell})} \tag{7}$$

Here, λ and l are the water content and thickness of the membrane, respectively.

The volume of water generation V_{wg} can be obtained as follows,

$$V_{wg} = \int_0^t \frac{P_e}{2V_c F} \tag{8}$$

which, V_{wg} is the total volume of water generated for t seconds; P_e is the output power with the unit of W, V_c is the voltage with the unit of V, and F is the Faraday constant with the value of 96485.33289 C/mol.

The value of parameter was chosen depending on the assembled PEMFC stack and is given in Table 2. The theoretical and experimental polarization curves of the assembled PEMFC stack are showed in Figure 4. The theoretical data are in good agreement with the measured voltage.

Table.2 Parameters for theoretical model of the assembled PEMFC

Symbols	Parameters	Values	Ref
ξ_1	/	-0.948	[44]
ξ_3	/	7.6×10^{-5}	[44]
ξ_4	/	-1.93×10^{-4}	[44]
$p^*_{H_2}$(atm)	/	0.6	-----
$p^*_{O_2}$(atm)	/	0.6	-----
A_C (m^2)	Cell area	500×10^{-4}	-----
δ_m(m)	Membrane thickness	25×10^{-6}	-----
R($J\cdot mol^{-1}\cdot K^{-1}$)	Universal gas constant	8.314	[44]
F(C·mol-1)	Faraday constant	96485	[44]
λ	Membrane resistivity parameter	12.5	[44]

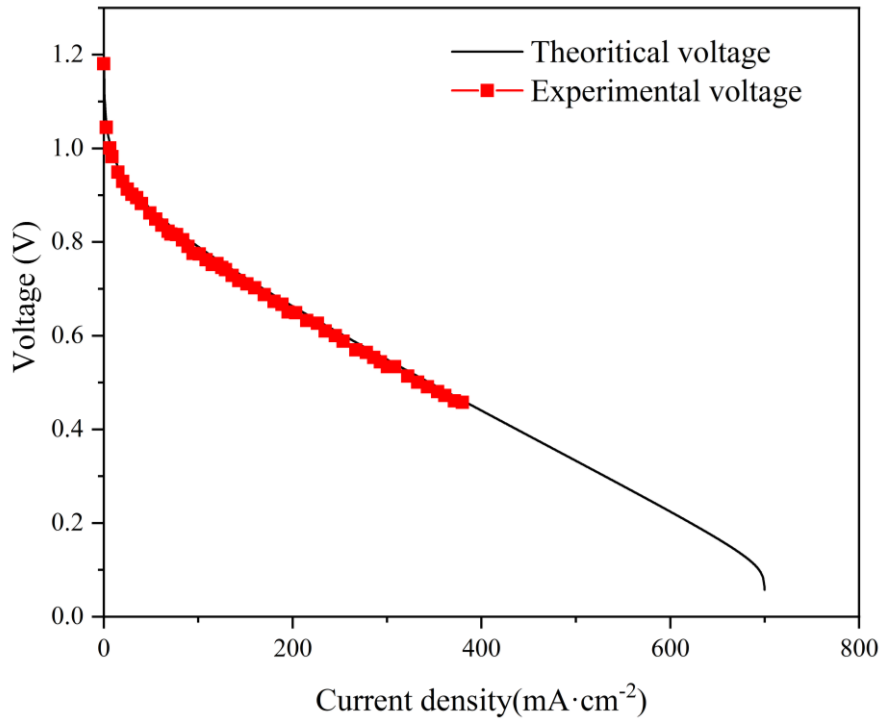

Figure 4. Comparison of theoretical and experimental polarization curves of the

assembled PEMFC stack

3. Results and Discussion

3.1 Effect of current density

To further improve the fuel utilization, the valves at the bottom of the buffer tank were kept closed at all time during operation, while the solenoid valves at the buffer tanks were opened after every 600 s of operation (t_p=600 s) with a purging pressure limit of 0.25 bar (P_l=0.25 bar). Figure 5(a) shows the dynamic characteristics of the PEMFC stack within the purge cycles operating at 65°C under a current density of 150 mA·cm^{-2} and 200 mA·cm^{-2}. After the first 600 s of operation, the voltage at the current density of 150 mA·cm^{-2} dropped from 0.685 V to 0.625 V, then returned to approximately 0.68 V. The voltage at the current density of 200 mA·cm^{-2} dropped from 0.63 V to 0.55 V, then returned to 0.68 V. The recovery of voltage and output power after the first cycle were 0.071 V and 35.5 W, respectively, for the current density of 150 mA·cm^{-2} and 0.112 V and 111.6 W, respectively, for the current density of 200 mA·cm^{-2}. It can be observed that before purging, the voltage continued to decrease due to the accumulation of water, but increased again because of the fresh fuel flowing into the stack in addition to the re-pressurizing of the anode after the closure of the purge valve [39]. The effects of purging demonstrated a high recovery percentage of voltage loss, especially at a higher current density (the percentage of voltage recovery was approximately 18%), indicating that the positive impact of purging is more obvious under higher current densities. What's more, there was no external emission during entire operating procedure in this DEAC mode to improve the hydrogen and oxygen utilization to 100%

which is greatly higher than that of other methods in Table 3.

Table 3. Comparison of the utilization of reactants of PEMFC

Methods	H2 utilization	O2 utilization	Mode	Ref
Multi-staged gas supply	99.6%	-----	DEA	[34]
Ejector	100%	-----	DEA	[40]
Compressor	-----	95%	DEC	[36]
Recirculation pump	-----	88.46%	DEC	[45]
Recirculation pump	88.5%	62.5%	DEAC	[46]
Our method	100%	100%	DEAC	-----

The voltage distribution for the stack under the current densities of 150 $mA \cdot cm^{-2}$ and 200 $mA \cdot cm^{-2}$ is shown in Figure 5(b). The average voltages for the stack under 150 $mA \cdot cm^{-2}$ (black dashed line) and 200 $mA \cdot cm^{-2}$ (red dashed line) are 0.692 V and 0.6172 V, respectively. The voltage distribution is more uniform for the current density at 150 $mA \cdot cm^{-2}$ (with a standard deviation of 33.9 mV) than for the current density of 200 $mA \cdot cm^{-2}$ (with a standard deviation of 54.6 mV).

The relationship between the average voltage and pressure variations of the designed DEAC system is shown in Figures 5(c) and (d). When the operating time reached 600 s, the solenoid valves placed at the inlet of the oxygen and hydrogen tanks were closed, indicating that the hydrogen and oxygen consumed in the stack were from the stored gas in the buffer tanks. Hence, the pressure continued to decrease until it reached P_l but there was no obvious drop in the voltage because there were residual reactants in the reactant interface during the short time. Then, the gas supply was switched back to the

stable and fresh gas through forced convection produced by the pressure difference due to gas purging to remove water, contributing to the voltage recovery. In Figure 5(c), the pressure differences under the current density of 150 $mA \cdot cm^{-2}$ at the hydrogen inlet, hydrogen buffer tank outlet, oxygen inlet, and oxygen buffer tank outlet are 0.41 bar, 0.4 bar, 0.15 bar, and 0.16 bar, respectively. In Figure 5(d), the pressure differences under the current density of 200 $mA \cdot cm^{-2}$ at the hydrogen inlet, hydrogen buffer tank outlet, oxygen inlet, and oxygen buffer tank outlet are 0.294 bar, 0.288 bar, 0.062 bar, and 0.062 bar, respectively. Liquid water can be easily removed from the channels to the buffer tanks by convection caused by the purging pressure difference. Although the purging pressure difference is beneficial for the performance of the PEMFC, the voltage cannot be completely recovered because it is slightly lower than the voltage in the previous cycle, especially for the current density of 200 $mA \cdot cm^{-2}$. Under the same purging pressure differences, the performance of the PEMFC at the current density of 150 $mA \cdot cm^{-2}$ is higher than that of 150 $mA \cdot cm^{-2}$ owing to the higher amount of water generated and accumulated in the channels under higher current densities.

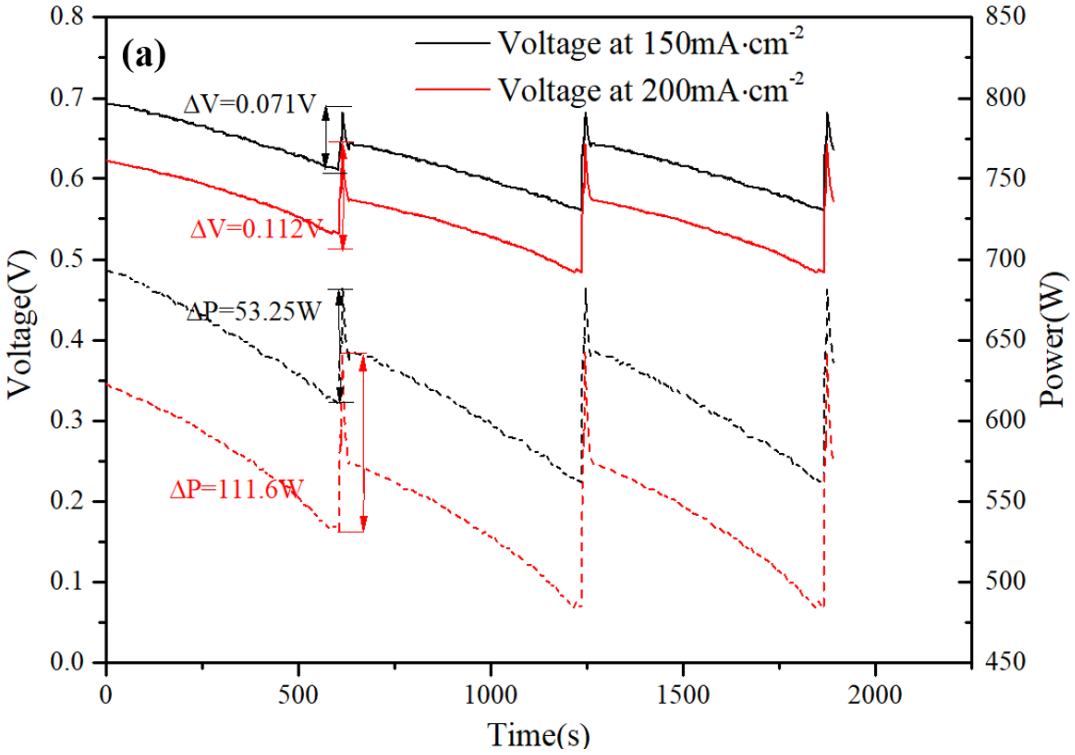
(a)
Voltage at 150mA·cm-2
Voltage at 200mA·cm-2
ΔV=0.071V
ΔV=0.112V
ΔP=53.25W
ΔP=111.6W
Voltage(V)
Power(W)
Time(s)
0.0
0.1
0.2
0.3
0.4
0.5
0.6
0.7
0.8
450
500
550
600
650
700
750
800
850
0
500
1000
1500
2000

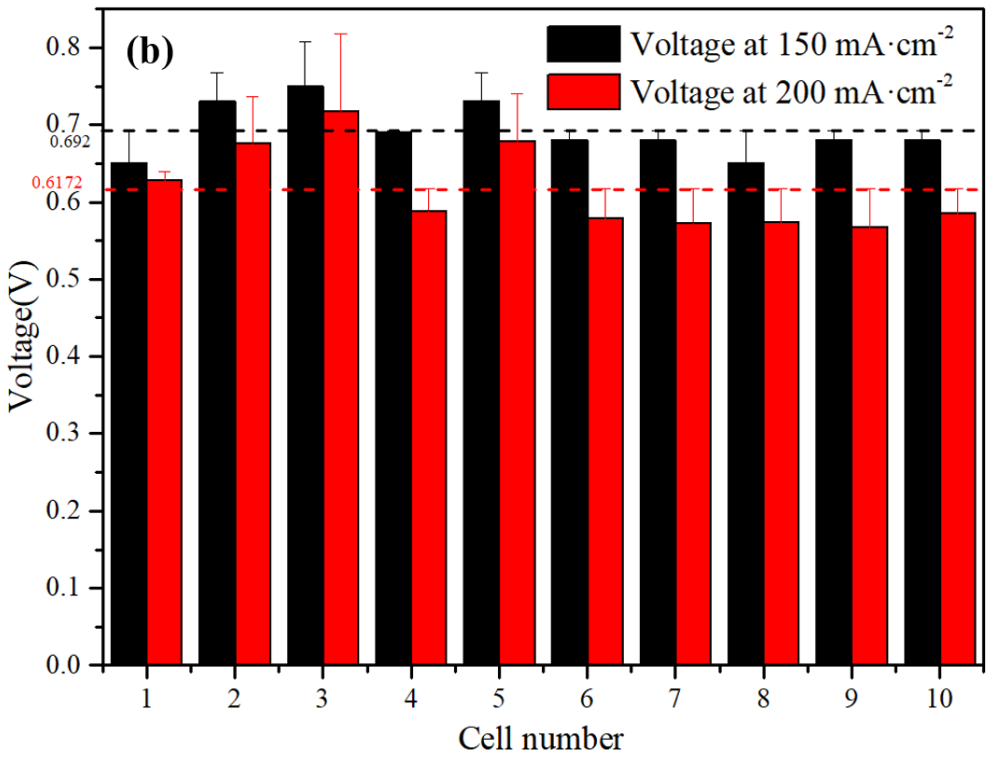
(b)
Voltage at 150 mA·cm-2
Voltage at 200 mA·cm-2
0.692
0.6172
Voltage(V)
Cell number
0.0
0.1
0.2
0.3
0.4
0.5
0.6
0.7
0.8
1
2
3
4
5
6
7
8
9
10

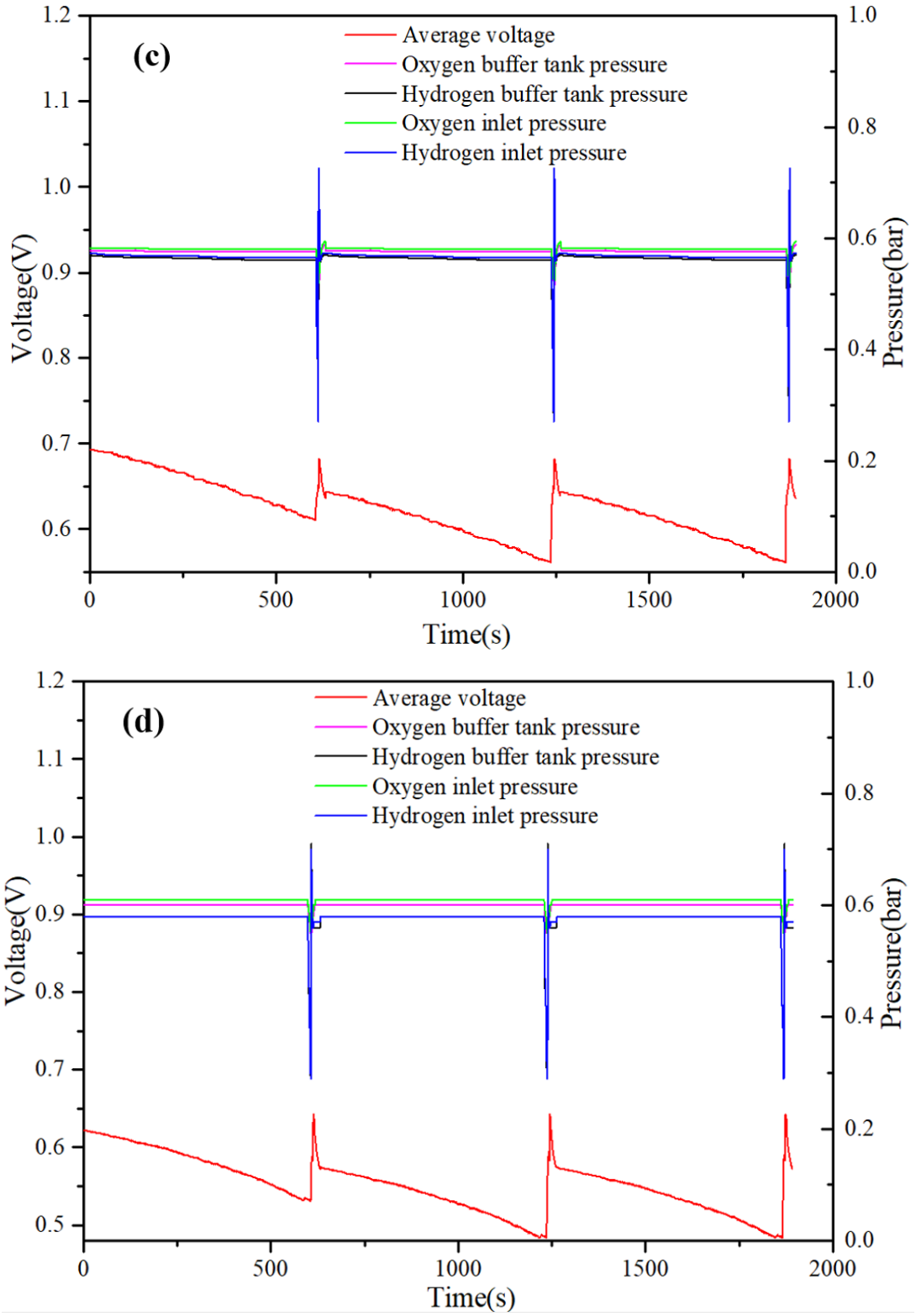

Figure 5. (a) Voltage and power variation of PEMFC stack under different current densities. (b) Voltage distribution of single cells. (c) Voltage and pressure variations at 150 mA·cm^{-2}. (d) Voltage and pressure variations at 200 mA·cm^{-2}.

3.2 Effects of pressure difference

Figure 6 shows the output dynamics of the system under different purging pressures (P_l =0.1 bar, P_l=0.2 bar, P_l=0.25 bar) at the current density of 150 mA·cm^{-2} and a temperature of 65°C for the voltage variations, water generation, and pressure variations. Figure 6(a) shows the output characteristics of three cycles in which the voltage decreases first and then increases in each cycle. As mentioned in section 3.1, the decrease in voltage was due to the accumulation of water. When the pressure drops to P_l, the gas supply switches back to using the stable fuel supply, causing a sharp increase in voltage due to the water removal caused by the pressure difference and the increase in pressure. Based on Equation (1), the pressure played an important role in the voltage variations. The performance of the PEMFC in cycle 1 for different conditions is the same in the purging intervals but there were differences in performance between the purging durations when gas purging was conducted. The voltage of the PEMFC at a purging pressure of 0.1 bar maintained a relatively stable value in each cycle as a result of efficient water removal under a large pressure difference whereas the voltage of the PEMFC at a purging pressure of 0.2 bar or 0.25 bar did not return to the initial value. Figures 5(c–e) show the relationship between the average voltage and the pressure variations under different purging pressure limits. The recovered voltage under the anode purging pressure of 0.1 bar is higher than that for 0.2 bar and 0.25 bar, indicating that the larger the pressure difference, the more voltage is recovered when considering the lower viscosity of the richer recirculated gas. The forced convection produced to remove water can be enhanced by improving the pressure difference and,

thereby, mitigate flooding in the cathode and anode and enhance mass transfer. Furthermore, a longer duration was needed to reach a lower purging pressure, indicating that the overall temperature and humidity of the recirculated gas were slightly higher, benefiting membrane hydration [39]. However, the pressure difference cannot be maximized without limits because fuel starvation will occur with the decrease in pressure and the power output will be too low to satisfy the power needs of external energy consumers.

Figure 5(b) shows the volume of liquid water under different purging pressures collected in the two buffer tanks within one cycle after 600 s of operation. The data represents the volume of water in the cathode and anode buffer tanks after 600 s of operation and the red dashed line is the theoretical volume of water. It can be observed that the sum of water collected in the two tanks operating at the anode purging pressure of 0.1 bar, 0.2 bar, 0.25 bar, and 0.3 bar is 95 mL, 92.5 mL, 91.3 mL, and 90.7 mL, respectively, values of which are very close to but less than the theoretical volume of 96 mL calculated by Equation (2). The difference in volume between the actual and theoretical water is due to the residual water in the stack and the walls of the pipeline. The difference in the volume of the collected water is due to various pressure differences caused by gas purging. The uniformity of the local current density can be improved and part of the generated water can continuously be removed with the help of gravity using vertical placements [25]. With the advantages of gas purging and the use of vertical placements, almost all of the generated water can be completely collected in the two buffer tanks. With the decrease in purging pressure, the pressure difference

increases and the volume of water collected increases as well. The anode and cathode purging pressure differences are 0.47 bar and 0.1 bar, 0.37 bar and 0.08 bar, and 0.295 bar and 0.05 bar, respectively, for three cycles. Although the pressure differences in the cathode are lower than those in the anode, the increase in the volume of water collected in the oxygen tank is higher than that in the hydrogen tank when the pressure difference increases, indicating that flooding is more serious in the cathode. The cathode pressure is higher than the anode pressure at all times to enhance water transportation from the cathode to the anode by back diffusion, thereby suppressing the occurrence of water flooding in the cathode. Additionally, water transportation by back diffusion can humidify dry hydrogen in the anode, accelerating the mass transfer and achieving better performance[47].

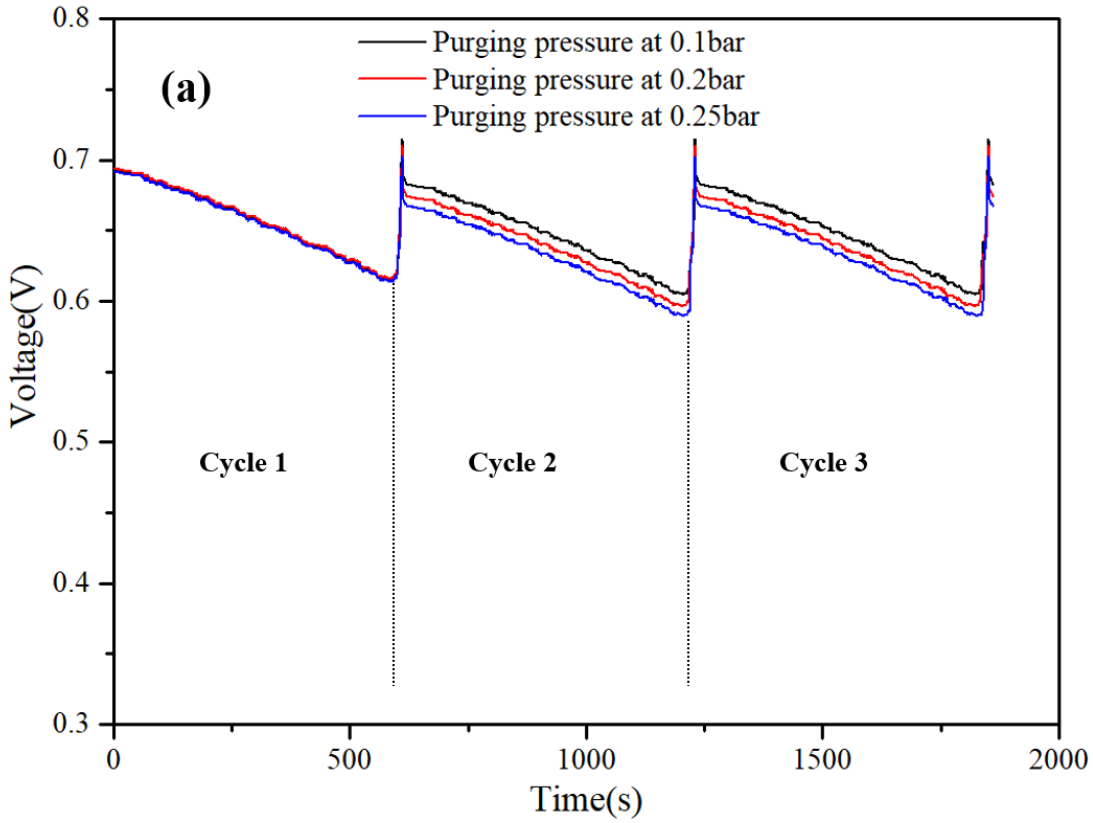

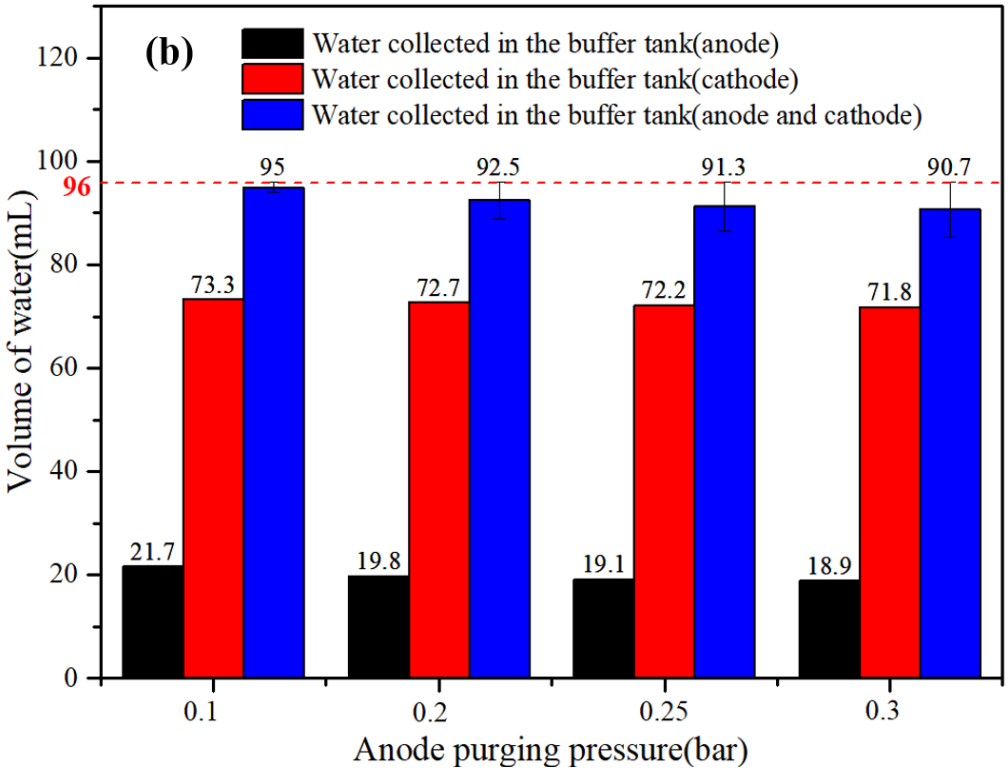
(b)
Water collected in the buffer tank(anode)
Water collected in the buffer tank(cathode)
Water collected in the buffer tank(anode and cathode)
Volume of water(mL)
Anode purging pressure(bar)
96
95
92.5
91.3
90.7
73.3
72.7
72.2
71.8
21.7
19.8
19.1
18.9
0.1
0.2
0.25
0.3

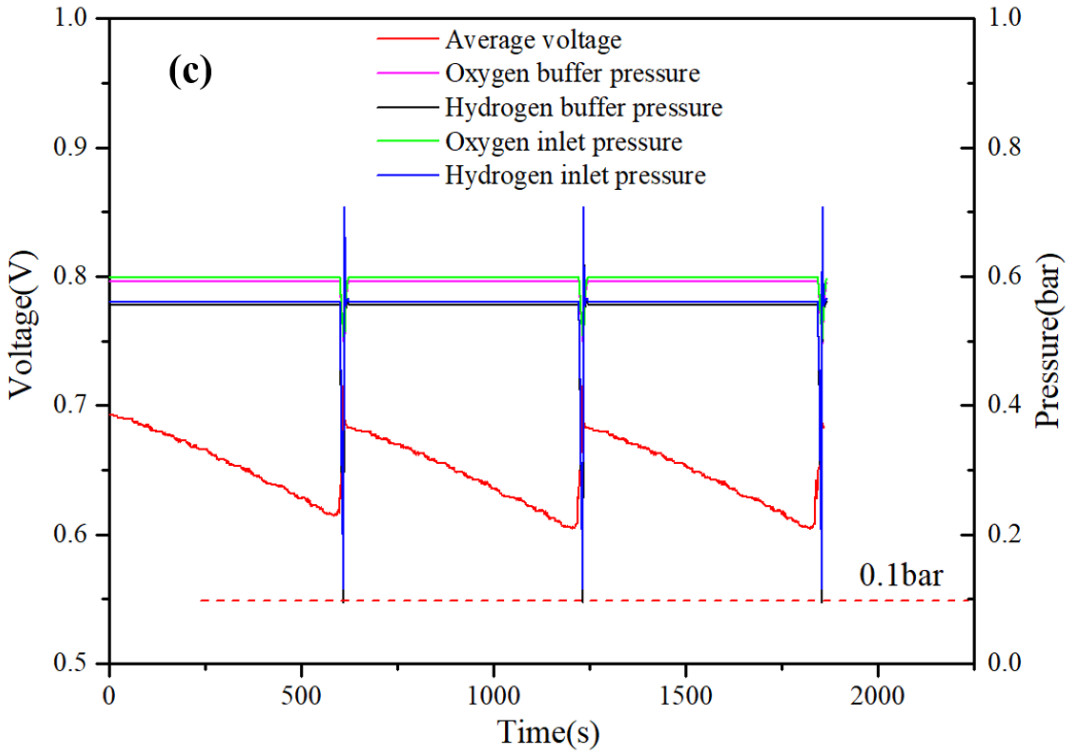
(c)
Average voltage
Oxygen buffer pressure
Hydrogen buffer pressure
Oxygen inlet pressure
Hydrogen inlet pressure
Voltage(V)
Pressure(bar)
Time(s)
0.1bar

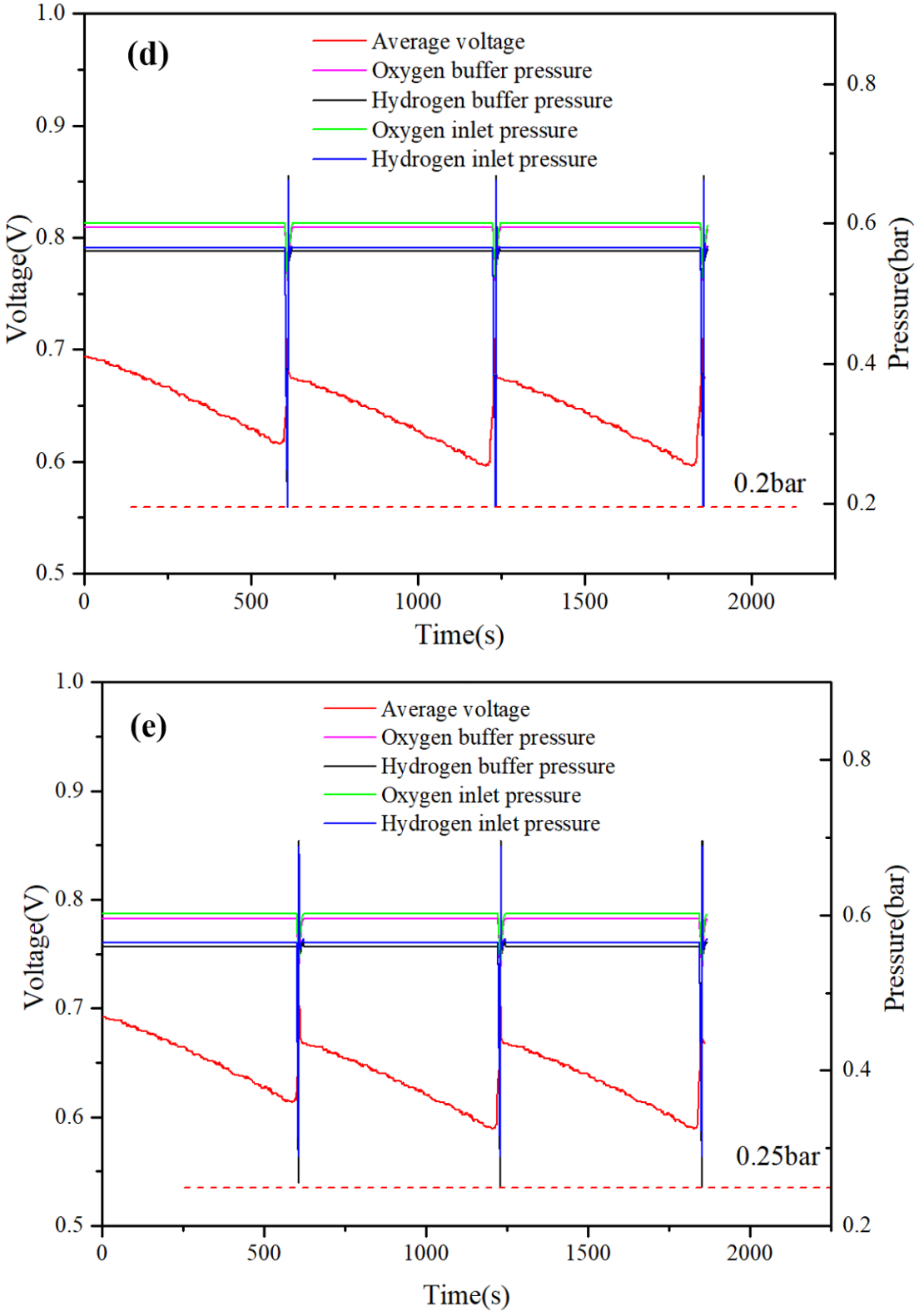

Figure 6. (a) Voltage and power variations of PEMFC stack under different purging pressures. (b) Water collected under different purging pressures. (c) Voltage and pressure variations at 0.1 bar. (d) Voltage and pressure variations at 0.2 bar. (e) Voltage

and pressure variations at 0.25 bar.

3.3 Effects of purging interval

Figure 7 shows the dynamic response of the system under different purging intervals operating at 65°C with the current density of 150 mA·cm^{-2}. In Figure 7(a), the voltage with t_p=100 s completely returns to initial values periodically while there exist unrecoverable losses in t_p=500 s and t_p=600 s. The purging duration lasts approximately 10 s and consumes 10%, 2%, and 1.67% of the purging period at t_p=100 s, 500 s, and 600 s, respectively. The voltage recovered for purging intervals of 100 s, 500 s, and 600 s is 0.0134 V, 0.01577 V, and 0.01961 V, respectively. It can be observed that with the extension of the purging interval, the recovery of voltage decreased. For short purging intervals, the accumulated water is removed quickly and the performance of the PEMFC stack is efficiently recovered. For long purging intervals, as the reaction proceeds, increasing liquid water is generated and gradually adheres to the porous electrode pores and gas channels, resulting in a decrease in the effective electrochemical reaction area and an obvious voltage drop [48]. When the purging is performed, the liquid water attached to the surface of the membrane is partially removed and the gas mass transfer is enhanced up to a limit. Hence, decreasing the purging interval is beneficial for increasing the stability and performance of the PEMFC.

The pressure variations for the interval of 100 s, 500 s, and 600 s are shown in Figures 7(c–e), respectively. A limited convective force to remove a specific amount of water was produced by a specific pressure difference, but with the shorter purging intervals, the water accumulated in the channels was repeatedly removed to maintain stable

operation. An interesting phenomenon in the slight voltage decay after the instance of purging can be explained by the plug flow of recycled gas and fresh gas alternatingly passing through the stack and eventually forming a uniform mixture with high humidity. But before the formation of this uniform mixture, there is a momentary mismatch between the gas supply and consumption [49]. Different purging intervals have a significant influence on the recovery of performance. The experimental results show that the shorter the purging intervals, the smaller the effects of water flooding, rendering purging more effective. In particular, the voltage variations under the intervals of 100 s can be periodically repeated without obvious degradations of the voltage peak, demonstrating that the shorter intervals can efficiently promote the recovery of performance of the PEMFC by removing the accumulated water[50]. However, that doesn't mean it can be unlimited shorten the purging interval for irreversible mechanical damage will be happened in membrane, like cracks or defects[51, 52].

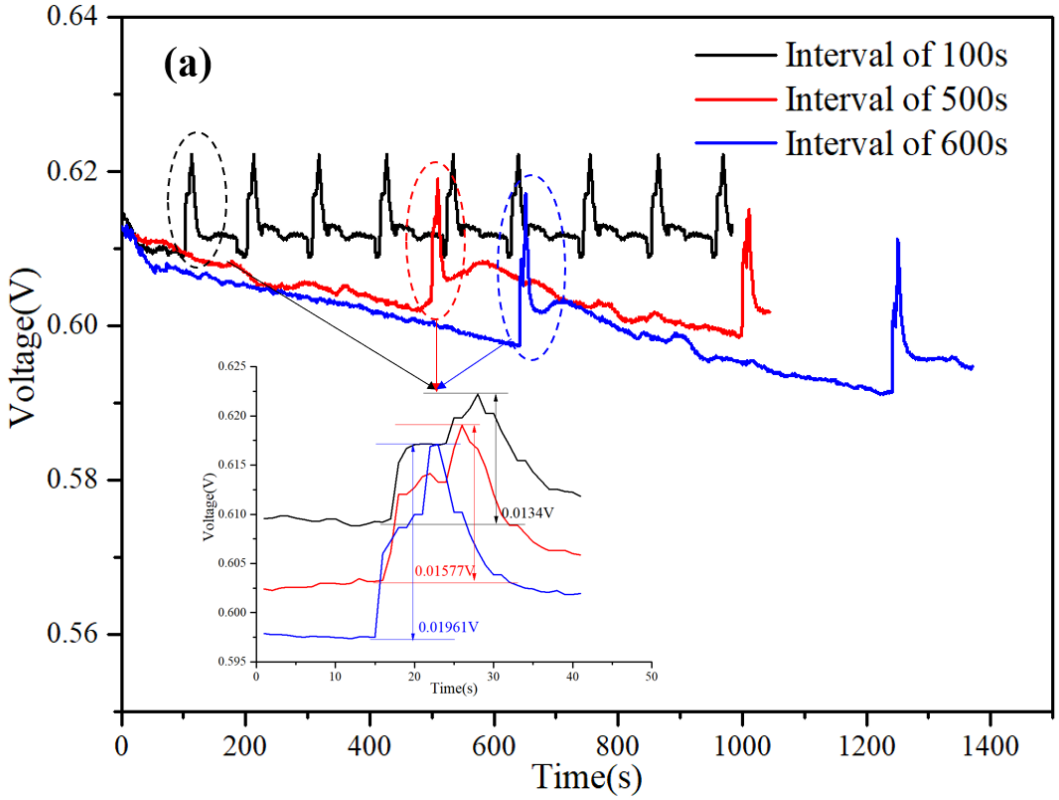
(a)
Interval of 100s
Interval of 500s
Interval of 600s
Voltage(V)
Time(s)
0.0134V
0.01577V
0.01961V

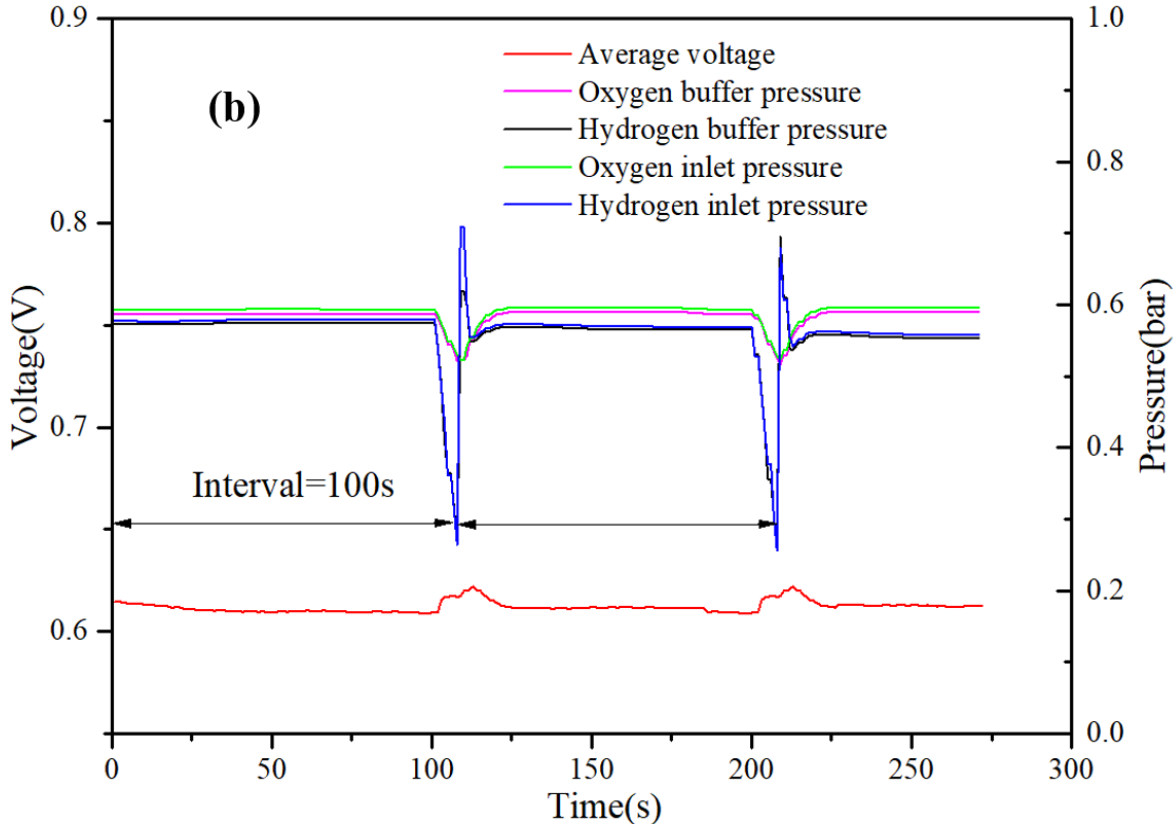
(b)
Average voltage
Oxygen buffer pressure
Hydrogen buffer pressure
Oxygen inlet pressure
Hydrogen inlet pressure
Interval=100s
Voltage(V)
Pressure(bar)
Time(s)

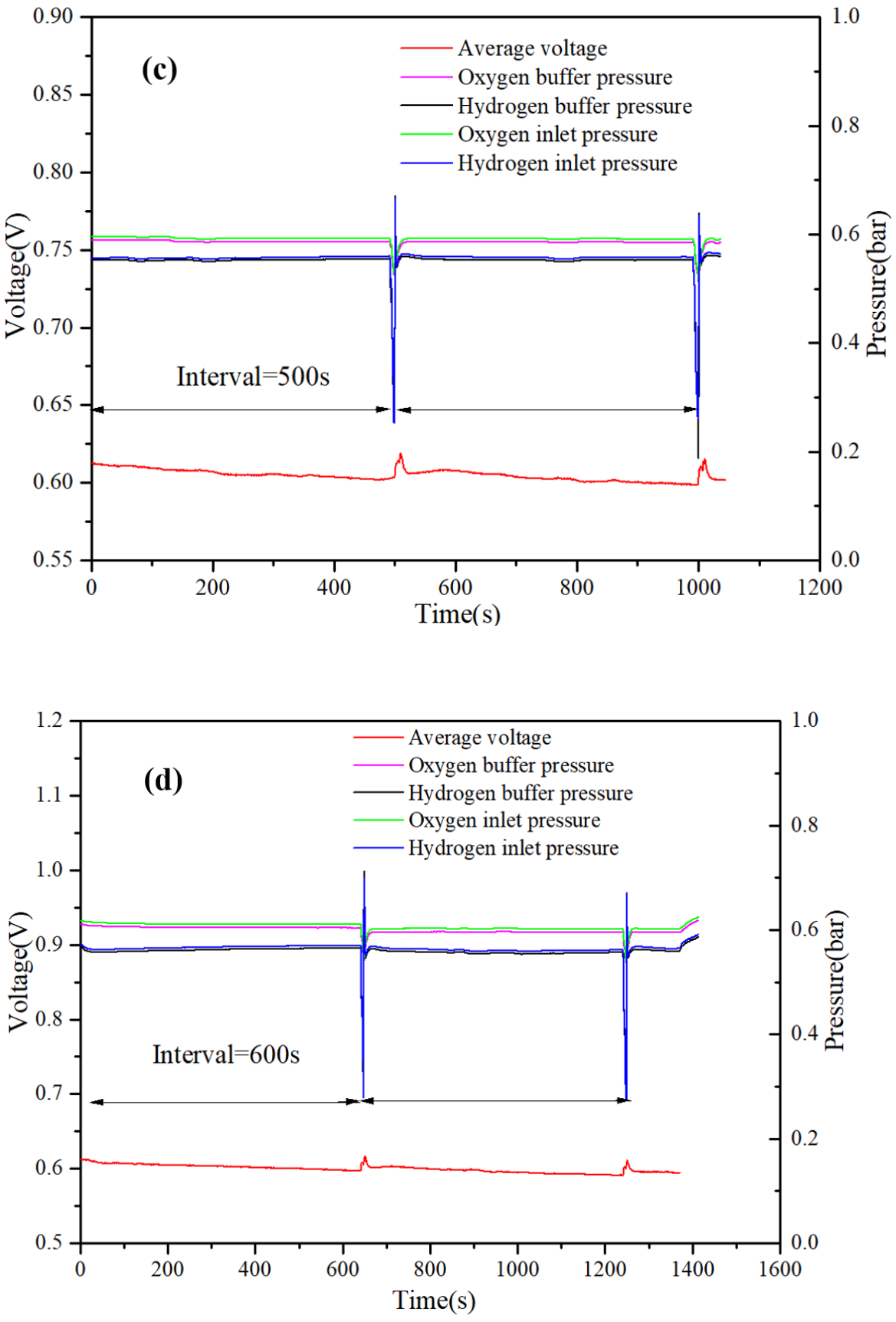

Figure 7. (a) Voltage and power variations of PEMFC stack under different purging

intervals. (b) Voltage and pressure variations with t_p=100 s. (c) Voltage and pressure variations with t_p=500 s. (d) Voltage and pressure variations with t_p= 600 s.

4. Conclusions

In this paper, a pressure-based purging strategy is proposed to study the effects of different operating conditions on the performance of a PEMFC with a dead-ended anode and cathode. A buffer tank at the outlet of the PEMFC is used to generate a pressure difference between the PEMFC and gas inlet when the purging strategy is applied. Liquid water can be removed effectively by the gas flow induced by the pressure difference during gas purging. The utilizations of hydrogen and oxygen can both reach 100% with the application of this strategy. A 10-single cell PEMFC stack with a dead-ended anode and cathode is fabricated to verify the effectiveness of this strategy. The following are our conclusions:

(1) Hydrogen and oxygen utilizations of this PEMFC stack with a dead-ended anode and cathode both increase to 100% without employing recirculation devices, and the stability of this system was verified during long-term operation.

(2) Particularly under a high current density, a large purging pressure difference provides a more powerful gas flow for water removal, which is used for the performance enhancement of the PEMFC.

(3) It is difficult to blow water out of the PEMFC when it gradually permeates into the micro/nano pores of the gas diffusion layer or catalyst layer. A decreased purging interval is beneficial for both water removal and the performance stability of the PEMFC.

Acknowledgement

This study was supported by the National Natural Science Foundation of China (Nos. 51776144, 52076096), Natural Science Foundation of Hubei Province (No. 2020CFA040) and Wuhan Applied Foundational Frontier Project (No. 2020010601012205).

References

[1] F. Huang, D. Qiu, S. Lan, P. Yi, L. Peng. Performance evaluation of commercial-size proton exchange membrane fuel cell stacks considering air flow distribution in the manifold. Energy Convers Manage. 2020;203:112256.

[2] X. Xu, W. Yang, X. Zhuang, B. Xu. Experimental and numerical investigation on effects of cathode flow field configurations in an air-breathing high-temperature PEMFC. Int J Hydrogen Energy. 2019;44:25010-25020.

[3] Y. Liu, W. Lehnert, H. Janßen, R.C. Samsun, D. Stolten. A review of high-temperature polymer electrolyte membrane fuel-cell (HT-PEMFC)-based auxiliary power units for diesel-powered road vehicles. J Power Sources. 2016;311:91-102.

[4] X. Lü, Y. Qu, Y. Wang, C. Qin, G. Liu. A comprehensive review on hybrid power system for PEMFC-HEV: Issues and strategies. Energy Convers Manage. 2018;171:1273-1291.

[5] I. Staffell. Zero carbon infinite COP heat from fuel cell CHP. Appl Energy. 2015;147:373-385.

[6] M. Bornapour, R.-A. Hooshmand, A. Khodabakhshian, M. Parastegari. Optimal stochastic scheduling of CHP-PEMFC, WT, PV units and hydrogen storage in

reconfigurable micro grids considering reliability enhancement. Energy Convers Manage. 2017;150:725-741.

[7] J. Han, J. Han, H. Ji, S. Yu. “Model-based” design of thermal management system of a fuel cell “air-independent” propulsion system for underwater shipboard. Int J Hydrogen Energy. 2020;45:32449-32463.

[8] C. Nuchturee, T. Li, H. Xia. Energy efficiency of integrated electric propulsion for ships – A review. Renew Sustain Energy Rev. 2020;134:110145.

[9] C.C. Chan. The State of the Art of Electric, Hybrid, and Fuel Cell Vehicles. Proceedings of the IEEE. 2007;95:704-718.

[10] B. Wang, D. Zhao, W. Li, Z. Wang, Y. Huang, Y. You, S. Becker. Current technologies and challenges of applying fuel cell hybrid propulsion systems in unmanned aerial vehicles. Progress in Aerospace Sciences. 2020;116:100620.

[11] X. Wang, J. Shang, Z. Luo, L. Tang, X. Zhang, J. Li. Reviews of power systems and environmental energy conversion for unmanned underwater vehicles. Renew Sustain Energy Rev. 2012;16:1958-1970.

[12] C. Li, D. Si, Y. Liu, J. Zhang, Y. Liu. Water management characteristics of electrospun micro-porous layer in PEMFC under normal temperature and cold start conditions. Int J Hydrogen Energy. 2020.

[13] O.S. Ijaodola, Z. El- Hassan, E. Ogungbemi, F.N. Khatib, T. Wilberforce, J. Thompson, A.G. Olabi. Energy efficiency improvements by investigating the water flooding management on proton exchange membrane fuel cell (PEMFC). Energy. 2019;179:246-267.

[14] H. Xue, L. Wang, H. Zhang, L. Jia, J. Ren. Design and investigation of multi-nozzle ejector for PEMFC hydrogen recirculation. Int J Hydrogen Energy. 2020;45:14500-14516.

[15] P.-H. Huang, J.-K. Kuo, W.-Z. Jiang, C.-B. Wu. Simulation analysis of hydrogen recirculation rates of fuel cells and the efficiency of combined heat and power. Int J Hydrogen Energy. 2020.

[16] S. Toghyani, E. Afshari, E. Baniasadi. A parametric comparison of three fuel recirculation system in the closed loop fuel supply system of PEM fuel cell. Int J Hydrogen Energy. 2019;44:7518-7530.

[17] Y. Yin, M. Fan, K. Jiao, Q. Du, Y. Qin. Numerical investigation of an ejector for anode recirculation in proton exchange membrane fuel cell system. Energy Convers Manage. 2016;126:1106-1117.

[18] J. Kang, D.W. Jung, S. Park, J.-H. Lee, J. Ko, J. Kim. Accelerated test analysis of reversal potential caused by fuel starvation during PEMFCs operation. Int J Hydrogen Energy. 2010;35:3727-3735.

[19] D. Lee, J. Bae. Visualization of flooding in a single cell and stacks by using a newly-designed transparent PEMFC. Int J Hydrogen Energy. 2012;37:422-435.

[20] K. Tajiri, C.-Y. Wang, Y. Tabuchi. Water removal from a PEFC during gas purge. Elec Acta. 2008;53:6337-6343.

[21] L.F. Arenas, G. Hadjigeorgiou, S. Jones, N. Van Dijk, D. Hodgson, A. Cruden, C. Ponce de León. Effect of airbrush type on sprayed platinum and platinum-cobalt catalyst inks: Benchmarking as PEMFC and performance in an electrochemical

hydrogen pump. Int J Hydrogen Energy. 2020;45:27392-27403.

[22] K. Nikiforow, P. Koski, J. Ihonen. Discrete ejector control solution design, characterization, and verification in a 5 kW PEMFC system. Int J Hydrogen Energy. 2017;42:16760-16772.

[23] F. Li, J. Du, L. Zhang, J. Li, G. Li, G. Zhu, M. Ouyang, J. Chai, H. Li. Experimental determination of the water vapor effect on subsonic ejector for proton exchange membrane fuel cell (PEMFC). Int J Hydrogen Energy. 2017;42:29966-29970.

[24] Z. Huang, Q. Jian, J. Zhao. Experimental study on improving the dynamic characteristics of open-cathode PEMFC stack with dead-end anode by condensation and circulation of hydrogen. Int J Hydrogen Energy. 2020;45:19858-19868.

[25] S. Liu, T. Chen, C. Zhang, Y. Xie. Study on the performance of proton exchange membrane fuel cell (PEMFC) with dead-ended anode in gravity environment. Appl Energy. 2020;261:114454.

[26] J.C. Kurnia, B.A. Chaedir, A.P. Sasmito, T. Shamim. Progress on open cathode proton exchange membrane fuel cell: Performance, designs, challenges and future directions. Appl Energy. 2021;283:116359.

[27] J. Zhao, Q. Jian, Z. Huang. Visualization study on enhancing water transport of proton exchange membrane fuel cells with a dead-ended anode by generating fluctuating flow at anode compartment. Energy Convers Manage. 2020;206:112477.

[28] B. Wang, K. Wu, Z. Yang, K. Jiao. A quasi-2D transient model of proton exchange membrane fuel cell with anode recirculation. Energy Convers Manage. 2018;171:1463-1475.

[29] J.W. Choi, Y.-S. Hwang, J.-H. Seo, D.H. Lee, S.W. Cha, M.S. Kim. An experimental study on the purge characteristics of the cathodic dead-end mode PEMFC for the submarine or aerospace applications and performance improvement with the pulsation effects. Int J Hydrogen Energy. 2010;35:3698-3711.

[30] M.R. Esbo, A.A. Ranjbar, S.M. Rahgoshay. Analysis of water management in PEM fuel cell stack at dead-end mode using direct visualization. Renewable Energy. 2020;162:212-221.

[31] B. Chen, J. Wang, T. Yang, Y. Cai, C. Zhang, S.H. Chan, Y. Yu, Z. Tu. Carbon corrosion and performance degradation mechanism in a proton exchange membrane fuel cell with dead-ended anode and cathode. Energy. 2016;106:54-62.

[32] B. Chen, Y. Cai, J. Shen, Z. Tu, S.H. Chan. Performance degradation of a proton exchange membrane fuel cell with dead-ended cathode and anode. Appl Therm Eng. 2018;132:80-86.

[33] J.C. Kurnia, A.P. Sasmito, T. Shamim. Advances in proton exchange membrane fuel cell with dead-end anode operation: A review. Appl Energy. 2019;252:113416.

[34] I.-S. Han, J. Jeong, H.K. Shin. PEM fuel-cell stack design for improved fuel utilization. International Journal of Hydrogen Energy. 2013;38:11996-12006.

[35] Q. Jian, L. Luo, B. Huang, J. Zhao, S. Cao, Z. Huang. Experimental study on the purge process of a proton exchange membrane fuel cell stack with a dead-end anode. Applied Thermal Engineering. 2018;142:203-214.

[36] S. Rodosik, J.P. Poirot-Crouvezier, Y. Bultel. Impact of humidification by cathode exhaust gases recirculation on a PEMFC system for automotive applications.

International Journal of Hydrogen Energy. 2019;44:12802-12817.

[37] A. Bozorgnezhad, M. Shams, H. Kanani, M. Hasheminasab, G. Ahmadi. The experimental study of water management in the cathode channel of single-serpentine transparent proton exchange membrane fuel cell by direct visualization. International Journal of Hydrogen Energy. 2015;40:2808-2832.

[38] M.M. Barzegari, M. Dardel, A. Ramiar, E. Alizadeh. An investigation of temperature effect on performance of dead-end cascade H2/O2 PEMFC stack with integrated humidifier and separator. International Journal of Hydrogen Energy. 2016;41:3136-3146.

[39] P. Koski, J. Viitakangas, J. Ihonen. Determination of fuel utilisation and recirculated gas composition in dead-ended PEMFC systems. Int J Hydrogen Energy. 2020;45:23201-23226.

[40] D. Jenssen, O. Berger, U. Krewer. Improved PEM fuel cell system operation with cascaded stack and ejector-based recirculation. Applied Energy. 2017;195:324-333.

[41] F. Jia, L. Guo, H. Liu. Dynamic characteristics and mitigations of hydrogen starvations in proton exchange membrane fuel cells during start-ups. Int J Hydrogen Energy. 2014;39:12835-12841.

[42] E. Alizadeh, M. Khorshidian, S.H.M. Saadat, S.M. Rahgoshay, M. Rahimi-Esbo. The experimental analysis of a dead-end H2/O2 PEM fuel cell stack with cascade type design. Int J Hydrogen Energy. 2017;42:11662-11672.

[43] Z. Wan, J. Liu, Z. Luo, Z. Tu, Z. Liu, W. Liu. Evaluation of self-water-removal in a dead-ended proton exchange membrane fuel cell. Appl Energy. 2013;104:751-757.

[44] M.J. Khan, M.T. Iqbal. Modelling and Analysis of Electro-chemical, Thermal, and Reactant Flow Dynamics for a PEM Fuel Cell System. Fuel Cells. 2005;5:463-475.

[45] Q. Zhang, Z. Tong, S. Tong. Effect of cathode recirculation on high potential limitation and self-humidification of hydrogen fuel cell system. Journal of Power Sources. 2020;468:228388.

[46] H. Jiang, L. Xu, C. Fang, X. Zhao, Z. Hu, J. Li, M. Ouyang. Experimental study on dual recirculation of polymer electrolyte membrane fuel cell. International Journal of Hydrogen Energy. 2017;42:18551-18559.

[47] B. Chen, Z. Tu, S.H. Chan. Performance degradation and recovery characteristics during gas purging in a proton exchange membrane fuel cell with a dead-ended anode. Appl Therm Eng. 2018;129:968-978.

[48] X. Ma, X. Zhang, J. Yang, W. Zhuge, S. Shuai. Impact of gas diffusion layer spatial variation properties on water management and performance of PEM fuel cells. Energy Convers Manage. 2021;227:113579.

[49] M. Steinberger, J. Geiling, R. Oechsner, L. Frey. Anode recirculation and purge strategies for PEM fuel cell operation with diluted hydrogen feed gas. Appl Energy. 2018;232:572-582.

[50] Y. Yang, X. Zhang, L. Guo, H. Liu. Local degradation in proton exchange membrane fuel cells with dead-ended anode. Journal of Power Sources. 2020;477:229021.

[51] P. Ren, P. Pei, Y. Li, Z. Wu, D. Chen, S. Huang. Degradation mechanisms of proton exchange membrane fuel cell under typical automotive operating conditions. Progress

in Energy and Combustion Science. 2020;80:100859.

[52] B. Chen, Y. Cai, Z. Tu, S.H. Chan, J. Wang, Y. Yu. Gas purging effect on the degradation characteristic of a proton exchange membrane fuel cell with dead-ended mode operation I. With different electrolytes. Energy. 2017;141:40-49.